Supporting Information for

Optimized molecular aggregation and photophysical process synergistically promoted photovoltaic performance in low-regularity benzo[*c*][1,2,5]-thiadiazole-based medium-bandgap copolymers *via* modulating π bridges

Junfeng Tong,[a,*] Yubo Huang,[a] Wuyan Liu,[a] Mengdie Shou,[a] Lili An,[b] Xuefeng Jiang,[a] Pengzhi Guo,[a] Yang Han,[c] Zezhou Liang,[d] Jianfeng Li[a] and Yangjun Xia[a,*]

[a]Gansu Provincial Engineering Research Center for Organic Semiconductor Materials and Application Technology, School of Materials Science and Engineering, Lanzhou Jiaotong University, Lanzhou, 730070, China.

[b]School of Chemical Engineering, Northwest Minzu University, Lanzhou 730030, China.

[c]School of Materials Science and Engineering, Tianjin University, Tianjin, 300072, China.

[d]Key Laboratory for Physical Electronics and Devices of the Ministry of Education & Shaanxi Key Lab of Information Photonic Technique, School of Electronics and Information Engineering, Xi′an Jiaotong University, Xi′an, 710049, China.

E-mail address: tongjunfeng139@163.com (J. Tong), xiayangjun2015@126.com.

Table S1 Bandgap, energy level and device parameters of the reported representative benzothiadiazole-based conjugated polymers.

Polymer donors	Acceptors	E_g^{opt} (eV)	E_{HOMO}/E_{LUMO} (eV)	V_{OC} (V)	J_{SC} (mA cm^{-2})	*FF* (%)	PCE (%)	Ref.
PTFBDT-BZS	IDIC	1.85	–5.43/–3.58	0.905	17.30	70.80	11.03	[1]
PBDTSF-FBT	ITIC	1.82	–5.41/–3.59	1.03	17.09	66.30	11.66	[2]
PBT-Cl	IT-4F	1.91	–5.51/–3.60	0.782	21.03	70.00	11.60	[3]
PBDT-AFBT	IDTCN-O	1.79	–5.35/–3.56	0.864	21.85	66.35	12.33	[4]
PffBT4T-C_9C_{13}	$PC_{71}BM$	1.65	–5.34/–3.69	0.788	20.20	74.00	11.70	[5]
PffBT4T-2OD	ZITI-N-EH	1.79	–5.30/–3.51	0.805	22.13	73.35	13.07	[6]
PhI-ffBT	IT-4F	1.75	–5.55/–3.80	0.91	19.41	76.00	13.31	[7]
2TRA	IEICO-4F	1.62	–5.27/–3.65	0.73	23.74	70.04	12.10	[8]
PffBT-T3(1,2)-2	$PC_{71}BM$	1.63	–5.31/–3.68	0.83	18.9	68.80	10.70	[9]
P3TEA	FTTB-PDI4	1.90	–5.46/–3.56	1.14	14.05	66.40	10.58	[10]

1. Experimental section

1.1. Materials and synthesis

All the available chemicals and solvents, unless otherwise specified, were purchased from Sigma-Aldrich Co., J&K, and Energy Chemical used without further purification. Electron acceptor (2,2′-((2*Z*,2′*Z*)-((12,13-bis(2-ethylhexyl)-3,9-diundecyl-12,13-dihydro[1,2,5]thiadiazolo-[3,4-*e*]thieno[2,"3′:4′,5′]thieno[2′,3′:4,5]pyrrolo[3,2-*g*]thieno[2′,3′:4,5]thieno[3,2-*b*]indole-2,10-di-yl)bis(methanylylidene))bis(5,6-difluoro-3-oxo-2,3-dihydro-1*H*-indene-2,1-diylidene))dimalono-nitrile) (Y6) and electron transfer material 3,3′-(1,3,8,10-tetraoxoanthra[2,1,9-*def*:6,5,10-*d′e′f′*]-diisoquinoline-2,9-(1*H*,3*H*,8*H*,10*H*)diyl)-bis(*N*,*N*-dimethylpropan-1-amine oxide) (PDINO) and 4,7-dibromobenzo[*c*][1,2,5]thiadiazole ($BTBr_2$) were purchased from Derthon Optoelectronic Materials Science Technology Co. LTD and SunaTech Inc., respectively. Chlorinated bistin 2,6-bis(trimethylstannane)-4,8-bis(4-chloro-5-(2-butyloctyl)thien-2-yl)benzo[1,2-*b*:4,5-*b*']dithiophene (ClBDTSn) was synthesized on the basis of reference.[11] Dibromides 4-bromo-7-(5-bromo-4-octyl-thien-2-yl)benzo[*c*][1,2,5]thiadiazole ($TBTBr_2$) and 4,7-di(5-bromo-4-octylthien-2-yl)benzo[*c*]-[1,2,5]thiadiazole ($DTBTBr_2$) were synthesized according to our reported method[12], and structures for all monomers were confirmed and characterized by ^{1}H NMR. The synthetic procedure for the medium band gap copolymers PClBDT-BT, PClBDT-TBT and PClBDT-DTBT were as follows.

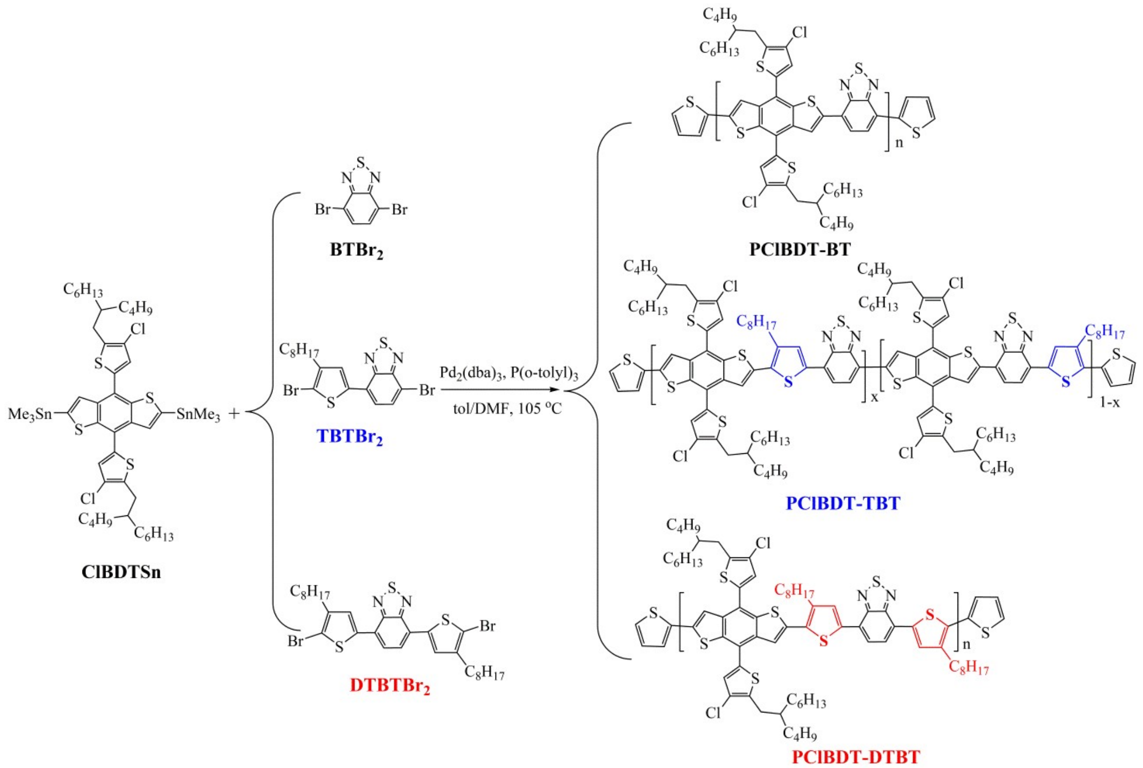

Scheme S1 Synthetic route for copolymers PClBDT-BT, PClBDT-TBT and PClBDT-DTBT.

1.1.1 2,6-Bis(trimethylstannane)-4,8-bis(4-chloro-5-(2-butyloctyl)thien-2-yl)benzo[1,2-*b*: 4,5-*b*']dithiophene (ClBDTSn)[11]

M.p., 122~125 ^{o}C. ^{1}H NMR (500 MHz, $CDCl_3$), δ (ppm): 7.62 (t, J = 14.5 Hz, 2H), 7.24 (s, 2H), 2.85 (d, J = 5.5 Hz, 4H), 1.80 (m, 2H), 1.40–1.30 (m, 32H), 0.90 (t, J = 7.0 Hz, 12H), 0.42 (t, J = 26 Hz, 18H). ^{13}C NMR (125 MHz, $CDCl_3$): 143.36, 143.23, 137.95, 137.30, 136.64, 130.57, 127.75, 122.53, 121.55, 39.38, 33.12, 31.90, 29.69, 28.84, 26.61, 23.05, 22.69, 14.17, 14.14. Alal. Calcd for $C_{48}H_{72}Cl_2S_2Sn_2$: C, 53.10%, H, 6.68%; Found: C, 54.00%; H, 6.51%.

1.1.2 4,7-Dibromobenzo[*c*][1,2,5]thiadiazole ($BTBr_2$)

M.p., 164~167 ^{o}C. ^{1}H NMR (400 MHz, $CDCl_3$): 7.73 (s, 2H). Alal. Calcd for $C_6H_2Br_2N_2S$: C, 24.51%, H, 0.69%, N, 9.53%; Found: C, 24.40%; H, 0.58%; N, 9.61%.

1.1.3 4-Bromo-7-(5-bromo-4-octylthien-2-yl)benzo[*c*][1,2,5]thiadiazole ($TBTBr_2$)[12]

M.p., 73~74 ^{o}C. ^{1}H NMR (400 MHz, $CDCl_3$), δ (ppm): 7.83 (d, J = 7.6 Hz, 1H), 7.75 (s, 1H), 7.62 (d, J = 7.6 Hz, 1H), 2.63 (t, J = 7.6 Hz, 2H), 1.67 (m, 2H), 1.40−1.25 (m, 10H), 0.88 (t, J = 6.4 Hz, 3H). Alal. Calcd for $C_{18}H_{20}Br_2N_2S_2$: C, 44.27%; H, 4.13%; N, 5.74%. Found C, 44.24%; H, 4.01%; N, 5.84%.

1.1.4 4,7-Di(5-bromo-4-octylthien-2-yl)benzo[*c*][1,2,5]thiadiazole ($DTBTBr_2$)[12]

M.p., 72~74 ^{o}C. ^{1}H NMR (400 MHz, $CDCl_3$), δ (ppm): 7.77 (s, 2H), 7.74 (s, 2H), 2.64 (t, 4H), 1.67 (m, 4H), 1.45−1.20 (m, 20H), 0.88 (t, 6H). Alal. Calcd for $C_{30}H_{38}Br_2N_2S_3$: C, 52.78%; H, 5.61%; N, 4.10%. Found C, 52.79%; H, 5.64%; N, 4.09%.

1.2 Syntheses of copolymers PClBDT-BT, PClBDT-TBT and PClBDT-DTBT

1.2.1 Poly[(4,8-bis(4-chloro-5-(2-butyloctyl)thien-2-yl)benzo[1,2-*b*:4,5-*b*']dithiophene-2,6-diyl) -*alt*-(benzo[*c*][1,2,5]thiadiazole-4,7-diyl)] (PClBDT-BT)[13]

Into a 25 mL two-neck round-bottom flask, carefully purified chlorinated bistin ClBDTSn (110.1 mg, 0.101 mmol), dibromide $BTBr_2$ (29.8 mg, 0.101 mmol), and 6 mL degassed toluene and 0.7 mL DMF was added, and the mixture was bubbled with Ar for another 20 min to remove O_2. And $Pd_2(dba)_3$ (1.0 mg), P(*o*-tolyl)$_3$ (2.0 mg) were added in one portion and the solution was bubbled with Ar for another 20 min. The mixture was vigorously stirred at 105 °C under Ar for 48 h. At the end of polymerization, the polymer was end-capped with 2-tributylstannylthiophene and 2-bromothiophene to remove bromo and trimethylstannyl end groups. Then, the mixture was poured into 300 mL methanol, and the polymer was precipitated and then collected by filtration. The crude polymer was purified by Soxhlet extraction with ethanol, acetone, hexane and toluene, respectively. The toluene fraction was condensed to approximately 6 mL and precipitated into methanol (300 mL). And the polymer PClBDT-BT was collected and dried under vacuum overnight as black solid (57.3 mg, yield: 63.3%). M_n = 19.0 kDa, polydisperse index (PDI = M_w/M_n): 1.7. ^{1}H NMR (400 MHz, o-DCB-d$_4$), δ (ppm), 7.90−7.30 (m, ArH), 3.30–2.70 (br, CH_2), 2.15−1.25 (m, CH, CH_2), 1.10−0.75 (m, CH_3). Anal. Calcd for $C_{48}H_{56}Cl_2N_2S_5$: C, 65.11%; H, 6.78%; N, 3.04%. Found, C, 65.01%; H, 6.61%; N, 3.22%.

1.2.2 Poly[(4,8-bis(4-chloro-5-(2-butyloctyl)thien-2-yl)benzo[1,2-*b*:4,5-*b*']dithiophene-2,6- diyl)-*co*-(7-(4-octylthien-2-yl)benzo[*c*][1,2,5]thiadiazole-4,5′-diyl)] (PClBDT-TBT)

A procedure similar to that of PClBDT-TBT was used with bistin ClBDTSn (109.6 mg, 0.101 mmol), $TBTBr_2$ (49.3 mg, 0.101 mmol). The title polymer was collected as black solid. (90.4 mg, yield: 83.0%). M_n = 22.3 kDa, PDI = 1.8. ^{1}H NMR (400 MHz, o-DCB-d$_4$), δ (ppm), 8.00−7.30 (m, ArH), 3.10–2.80 (br, CH_2), 2.10−1.25 (m, CH, CH_2), 1.10−0.75 (m, CH_3). Anal. Calcd for $C_{60}H_{74}Cl_2N_2S_6$: C, 66.32%; H, 6.86%; N, 2.58%. Found, C, 66.21%; H, 6.69%; N, 2.70%.

1.2.3 Poly[(4,8-bis(4-chloro-5-(2-butyloctyl)thien-2-yl)benzo[1,2-*b*:4,5-*b*']dithiophene-2,6-diyl-*alt*-4,7-di(3-octylthien-2-yl)benzo[*c*][1,2,5]thiadiazole-5,5′-diyl)] (PClBDT-DTBT)

A procedure similar to that of PClBDT-TBT was used with ClBDTSn (107.2 mg, 0.099

mmol), $DTBTBr_2$ (67.6 mg, 0.099 mmol). The polymer was collected as black solid. (128 mg, yield: 76.1%). M_n = 21.6 kDa, PDI = 1.8. ^{1}H NMR (400 MHz, o-DCB-d_4), δ (ppm), 8.16 (br, ArH, 2H), 7.91 (br, ArH, 2H), 7.76 (br, ArH, 2H), 7.48 (br, ArH, 2H), 3.02 (br, CH_2 of ClBDT, 4H), 2.93 (br, CH_2 of octylthienyl, 4H), 2.00−1.80 (m, CH, CH_2, 6H), 1.50−1.25 (m, CH_2, 52H), 0.95−0.85 (m, CH_3, 18H). Anal. Calcd for $C_{72}H_{92}Cl_2N_2S_7$: C, 67.51%; H, 7.24%; N, 2.19%. Found, C, 67.36%; H, 7.13%; N, 2.29%.

1.3 Measurement and characterization

^{1}H NMR spectra was measured on a Bruker 500 MHz AVANCE NEO (Rheinstetten, Germany) spectrometer, with tetramethylsilane (TMS) as the internal reference. Chemical shifts (δ) were recorded in units of ppm and their splitting patterns were designed as s (singlet), d (doublet), t (triplet), m (multiplet), and br (broaden). Note that *o*-dichlorobenzene-d4 (o-DCB-d4) residual peak was taken as internal reference at 7.20 ppm for ^{1}H NMR. Melting points were obtained on a microscopic melting point apparatus (Beijing Taike), and the temperature gauge was uncorrected. C, H and N elemental analyses (EAs) were carried out on a Vario EL Elemental Analysis Instrument (Elementar Co.). TGA curves were collected on a TGA 2050 instruments (New Castle, DE, USA) at the heating rate of 10 $^{o}C\cdot min^{-1}$ and under a N_2 flow rate (20 $mL\cdot min^{-1}$). UV-Vis absorption measurement was performed on a UV-1800 spectrophotometer (Shimadzu, Kyoto, Japan). Thin film X-ray diffraction (XRD) was recorded on a PANalytical X′Pert PRO diffractometer equipped with a rotating anode (Cu *K*α radiation, λ = 1.54056 Å). The electrochemical properties of films were measured on a CHI600D electro-chemical instrument (Chenhua, Shanghai, China) in anhydrous CH_3CN at a scan rate of 100 $mV\cdot s^{-1}$ under N_2. Tetra(n-butyl)ammonium hexafluorophosphate (Bu_4NPF_6) (0.1 $mol\cdot L^{-1}$) was utilized as the electrolyte. A three-electrode cell was used in all experimental, wherein glassy carbon electrode coated by polymer film, platinum wire and $Ag/AgNO_3$ (0.01 M of $AgNO_3$ in CH_3CN) electrode were used as the working, counter and reference electrode, respectively. The potential of $Ag/AgNO_3$ reference electrode was calibrated by the ferrocene/ferrocenium couple (Fc/Fc^+), whose energy level was –4.80 eV. Note that polymer′s thin films were obtained by dropcasting 1 μL studied material chlorobenzene solution with the concentration of 1 $mg\cdot mL^{-1}$ onto the glass carbon electrode, and then dried in the air. The contact angle was measured with an optical contact angle measuring and contour analysis systems (Dataphysics OCA 25). Atomic force microscopy (AFM) images were acquired on an MFP-3D-SA (Asylum Research, Santa Barbara, CA, USA) in a tapping mode. Transmission electron microscopy (TEM) images were obtained on a Tecnai G^2 F20 at accelerating voltage of 200 kV.

1.4 Fabrication of PSCs and mobility characterization

Indium tin oxide (ITO) coated glass substrates were washed by a wet-cleaning process inside an ultrasonic bath, with de-ionized water, acetone, de-ionized water and isopropanol in turn. After drying under nitrogen flow, the substrates were treated with oxygen plasma for 10 min, then a thin layer of poly(3,4-ethylenedioxythiophene):poly(styrene-sulfonate) (PEDOT:PSS, ca. 40 nm, Clevios PVP Al4083) was spin-coated onto the ITO substrates and annealed at 150 ºC for 20 min. After that the substrates were transferred into a nitrogen-filled glove box and the active layer was prepared. The active layer, with a thickness in the 100–120 nm range, was deposited on top of the PEDOT:PSS layer by spin-casting from chloroform solution containing the studied materials. The thickness of the active layer was verified by a surface profilometer (DektakXT, Bruker). Then, an ultrathin layer of PDINO (1 mg·mL^{-1} in methanol) was spin-coated on the active layer. Finally, the Al layer (~55 nm) as the cathode was thermally evaporated under a vacuum pressure of 10^{-4} Pa. Moreover, the all effective device area in this work was 0.1 cm^2, which was ascertained by a shadow mask. The thickness values of the evaporated Al were monitored by a quartz crystal thickness/ratio monitor (SI-TM206, Shenyang Sciens Co.). The PCEs of the resulting PSCs were measured under 1 sun, AM 1.5 G (Air mass 1.5 global) condition using a solar simulator (XES-70S1, San-EI Electric Co.) with irradiation of 100 mW·cm^{-2}. The current density-voltage (*J*-*V*) characteristics were recorded with a Keithley 2400 source-measurement unit. The spectral responses of the devices were measured with a commercial external quantum efficiency (EQE)/incident photon to charge carrier efficiency (IPCE) setup (7-SCSpecIII, Beijing 7-star Opt. In. Co.) equipped with a standard Si diode.

The hole-only and electron-only devices were prepared with a diode configuration of ITO/PEDOT:PSS/active layer/MoO_3/Ag or ITO/ZnO/active layer/PDINO/Ag, respectively. The device characteristics were extracted by modeling the dark current under an applied forward bias. The hole and electron mobilities of the active layers were extracted by fitting the current-voltage curves using the Mott-Gurney relationships[14] (space-charge-limited current, SCLC). The field dependent SCLC behavior can be expressed as: $J = \frac{9}{8}\varepsilon_0\varepsilon_r\mu\frac{V^2}{L^3}$. Where J stands for the current density, ε_0 is the permittivity of free space (8.85×10^{-12} F·m^{-1}), ε_r is the relative permittivity of the transport medium (assumed to be 3, which is a typical value for CPs), μ is the zero-field mobility of hole or electron, L is the thickness of the active layer, and effective voltage $V = (V_{appl} - V_{bi})$, where V_{appl} is the applied voltage to the device and V_{bi} is the built-in voltage. By linearly fitting $J^{1/2}$

with V, the mobilities were extracted from the slope and L: $\mu = \frac{slope^2 \times 8L^3}{9\varepsilon_0\varepsilon_r}$. For the hole-only devices, V_{bi} is 0 V, while V_{bi} = 0.7 V in the electron-only devices.

1.5 Surface energy calculation[15,16]

The surface tension (γ) can be evaluated using the Wu model, *via* Equations (1), (2), and (3), on the basis of the measured contact angles (θ) information.

$$\gamma_{water}(1 + cos\Theta_{water}) = \frac{4\gamma_{water}^{d}\gamma^{d}}{\gamma_{water}^{d} + \gamma^{d}} + \frac{4\gamma_{water}^{p}\gamma^{p}}{\gamma_{water}^{p} + \gamma^{p}} \quad (1)$$

$$\gamma_{EG}(1 + cos\theta_{EG}) = \frac{4\gamma_{EG}^{d}\gamma^{d}}{\gamma_{EG}^{d} + \gamma^{d}} + \frac{4\gamma_{EG}^{p}\gamma^{p}}{\gamma_{EG}^{p} + \gamma^{P}} \quad (2)$$

$$\gamma = \gamma^{d} + \gamma^{p} \quad (3)$$

Where, γ is the surface energy of the studied semiconductor; γ^d and γ^p are the dispersion and polar components of γ; γ^i is the total surface energy of the i material (i = water or ethylene glycol); γ_i^d and γ_i^p are the dispersion and polar components of γ_i; and θ is the droplet contact angle (water or ethylene glycol) on the semiconductor film. Flory−Huggins interaction parameter $\chi^{donor-acceptor}$, which is a parameter to evaluate the interaction between polymeric donors and acceptor Y6, based on this, the miscibility of the two components can be objectively judged. The smaller the difference of surface energy between donor and acceptor, the lower the value of $\chi^{donor-acceptor}$ and the better the miscibility.

1.6 Femtosecond time-resolved Transient Absorption (fs-TA) Measurements[17]

Fs-TA spectroscopy was performed to measure the temporal evolution of the absorption changes in the excited states, through which the carrier dynamics in femtosecond to nanosecond regime could be revealed. The laser beam is supplied by amplified Ti: sapphire laser source (800 nm, Coherent) that provides 100 fs pulses with a repetition rate of 1 kHz. The output was split into two beams, the stronger one of which was frequency doubled to generate a 400 nm pump light, and the other one was focused into a sapphire plate to generate a broadband supercontinuum probe light. Using an optical chopper, the repetition rate of the pump pulses was adjusted to 500 Hz, and was focused on the sample with the probe pulse (white light). The TA spectra were obtained by comparing the probe light spectra with and without pump light excitation. The photo-induced absorption change as a function of wavelength was described using optical density (absorbance) changes (ΔOD(λ)). By adjusting the delay time between the pump and probe pulses, a 3D transient spectral image ΔOD(λ,t) was formed.

2 Supplementary figures and tables

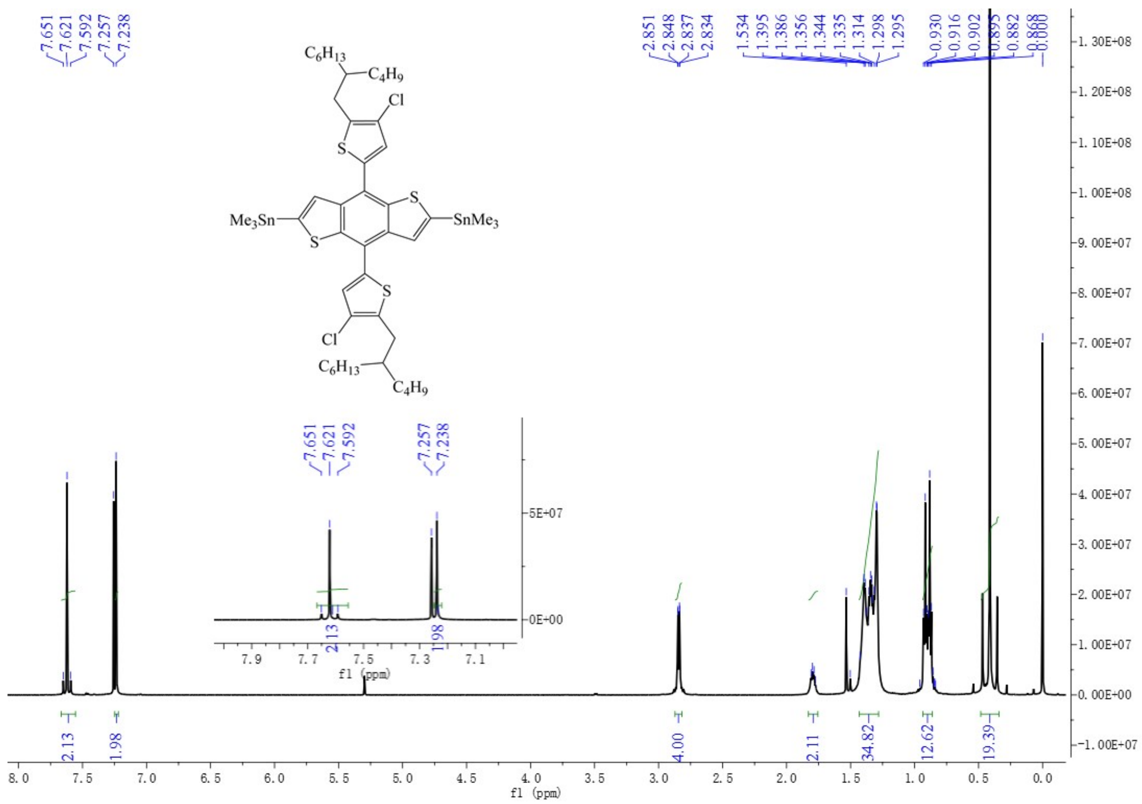

Fig. S1 ^{1}H NMR spectrum of ClBDTSn in $CDCl_3$.

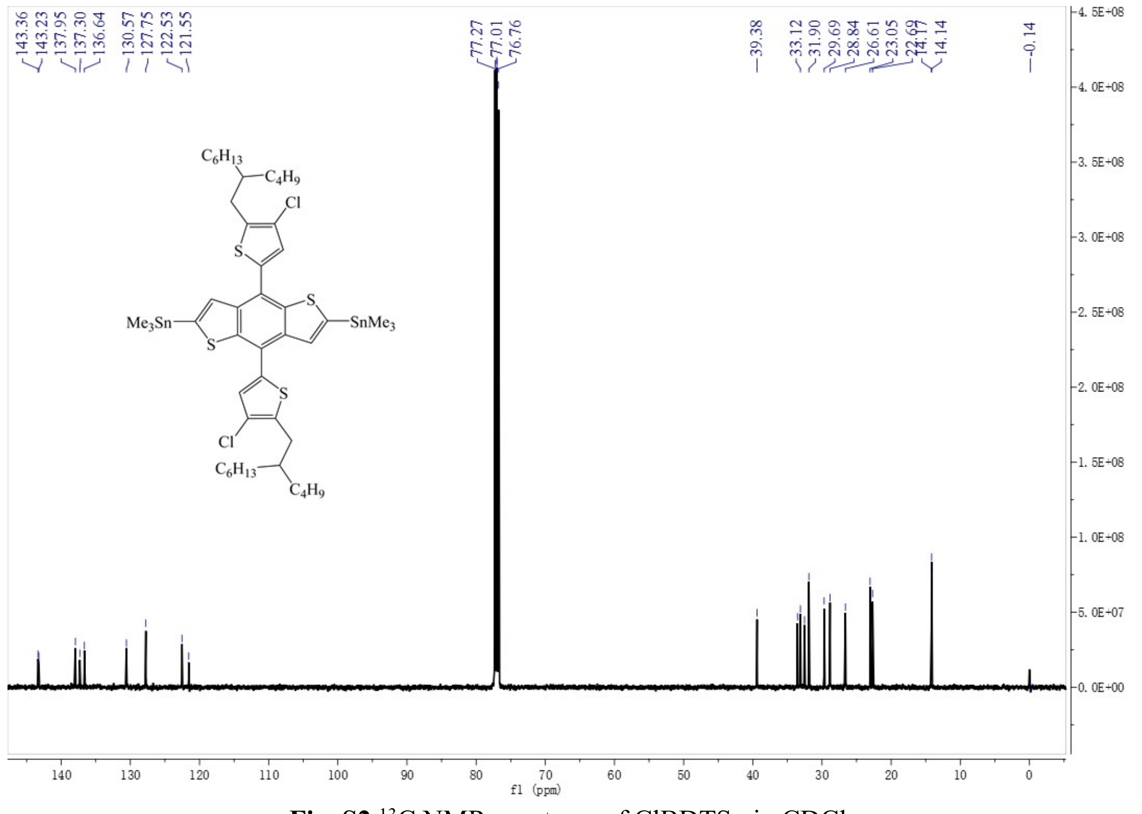

Fig. S2 ^{13}C NMR spectrum of ClBDTSn in $CDCl_3$.

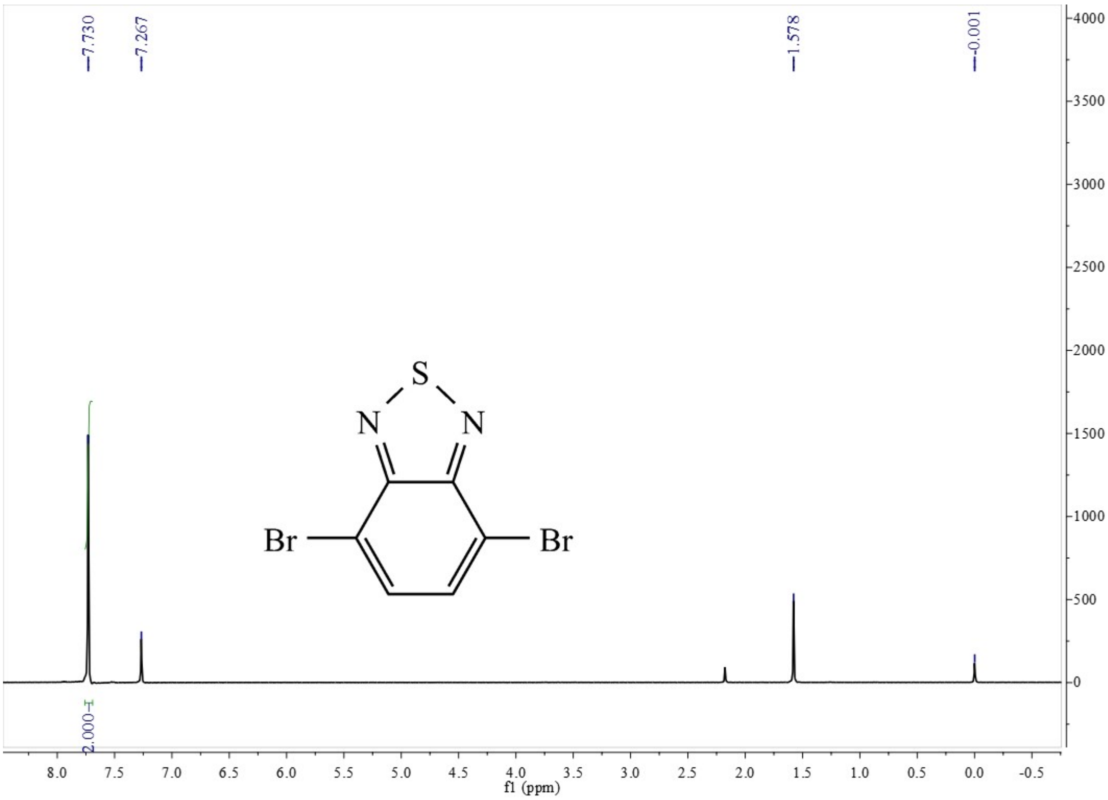

Fig. S3 ^{1}H NMR spectrum of $BTBr_2$ in $CDCl_3$.

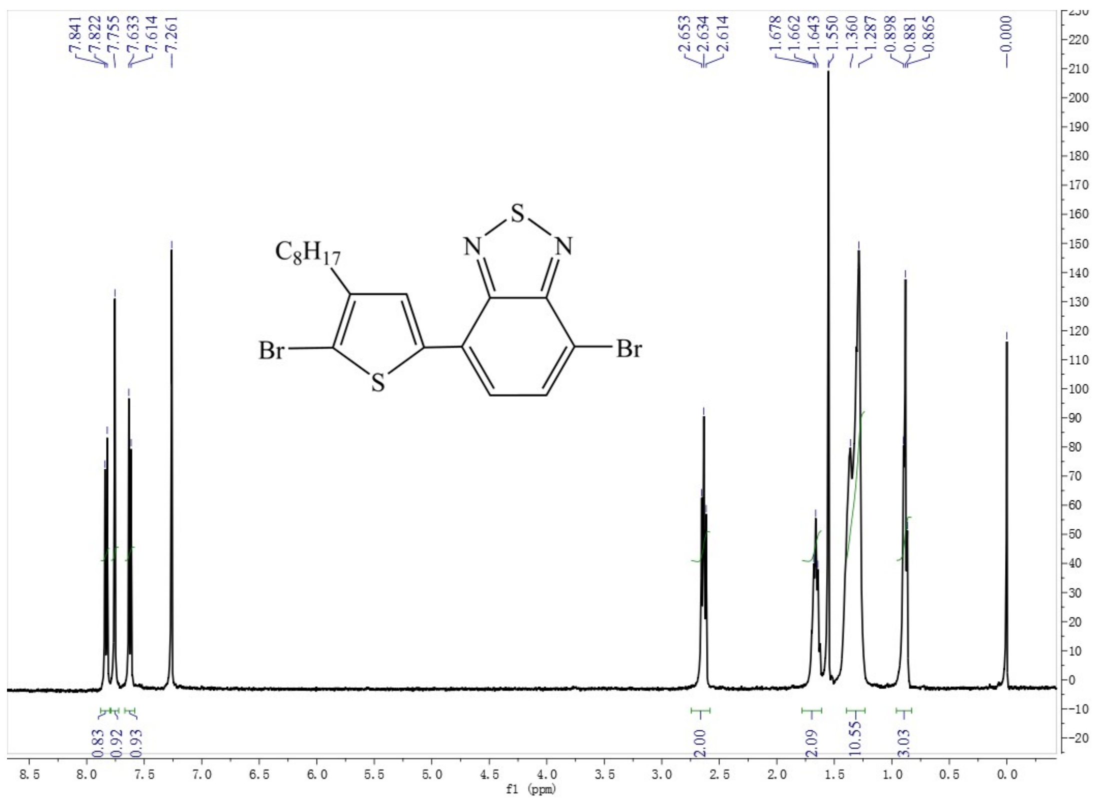

Fig. S4 ^{1}H NMR spectrum of $TBTBr_2$ in $CDCl_3$.

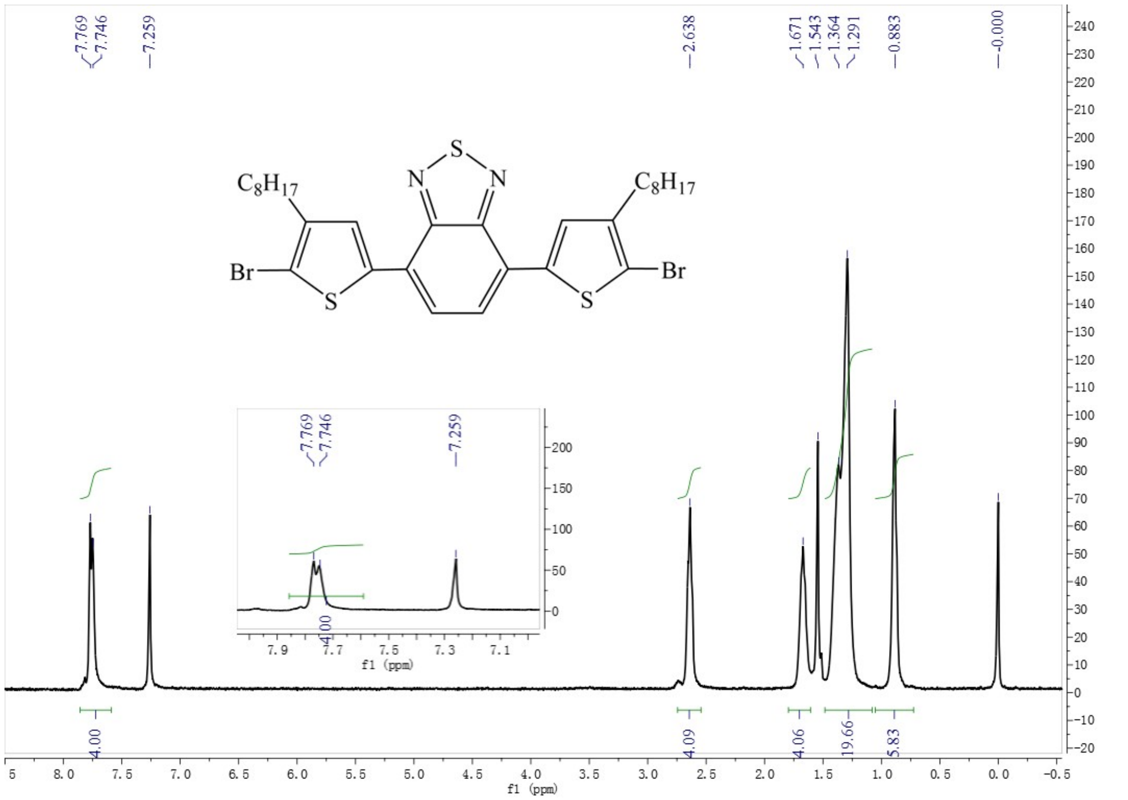

Fig. S5 ^{1}H NMR spectrum of $DTBTBr_2$ in $CDCl_3$.

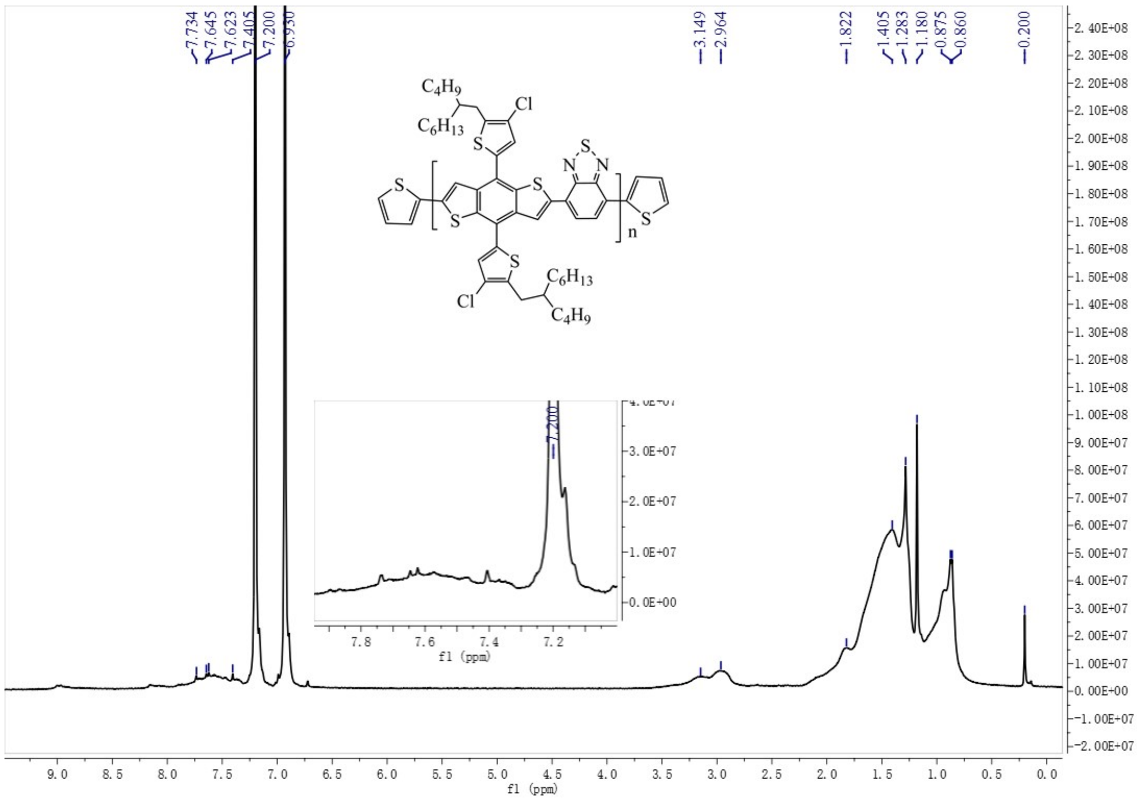

Fig. S6 ^{1}H NMR spectrum of PClBDT-BT *o*-DCB-d4 at 85 °C.

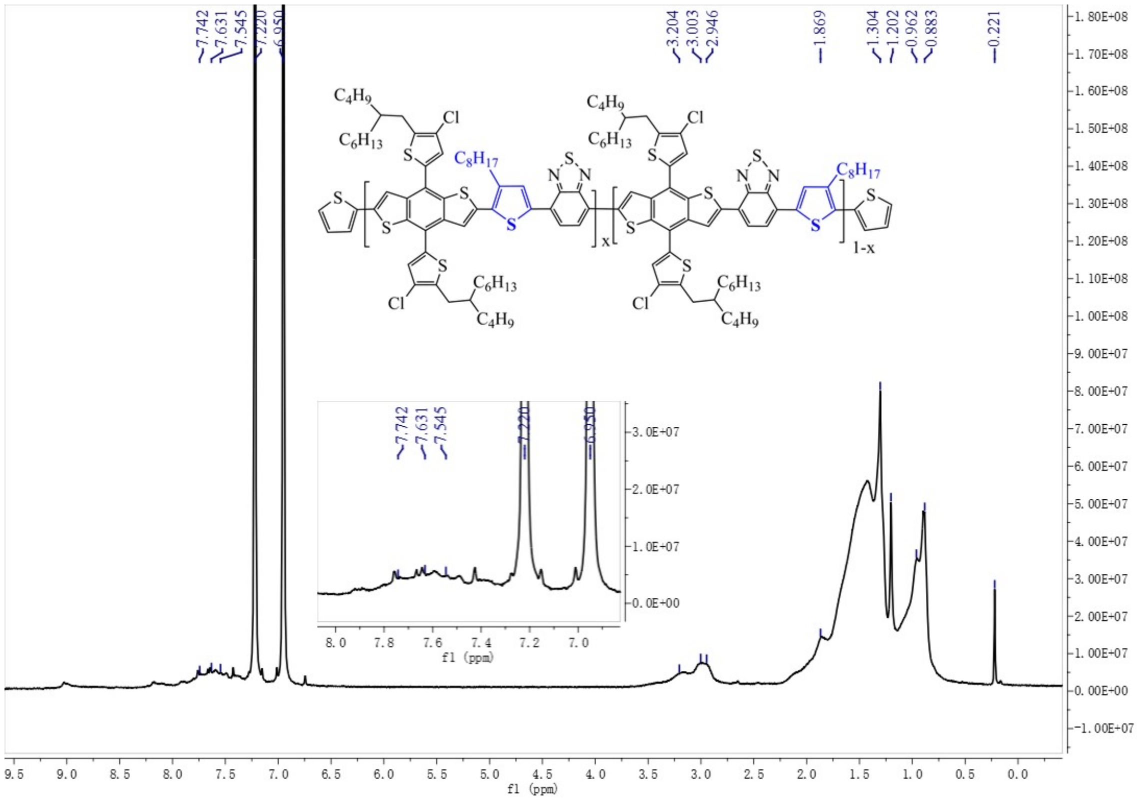

Fig. S7 [1]H NMR spectrum of PClBDT-TBT in *o*-DCB-d4 at 85 °C.

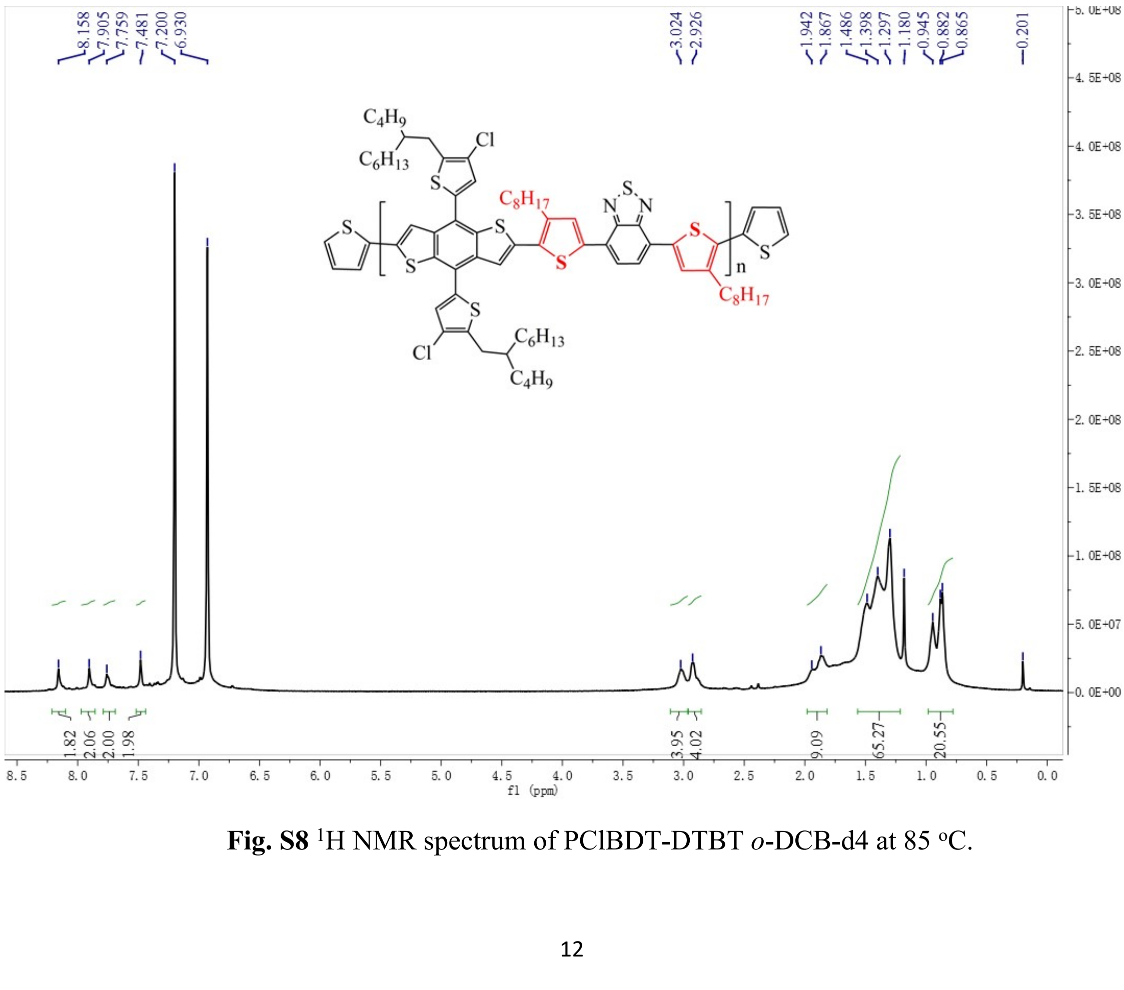

Fig. S8 [1]H NMR spectrum of PClBDT-DTBT *o*-DCB-d4 at 85 °C.

Table S2 Yield, molecular weight, TGA and absorption coefficients for the studied copolymers.

Polymer	Yield (%)	M_n (kDa)	M_w (kDa)	PDI	T_D (^oC)	ε_{soln} (M^{-1} cm^{-1})
PClBDT-BT	63.3	19.0	32.3	1.7	416	3.27×10^4 (λ = 639 nm)
PClBDT-TBT	83.0	22.3	40.1	1.8	371	3.24×10^4 (λ = 639 nm)
PClBDT-DTBT	76.1	21.6	38.9	1.8	386	3.58×10^4 (λ = 608 nm)

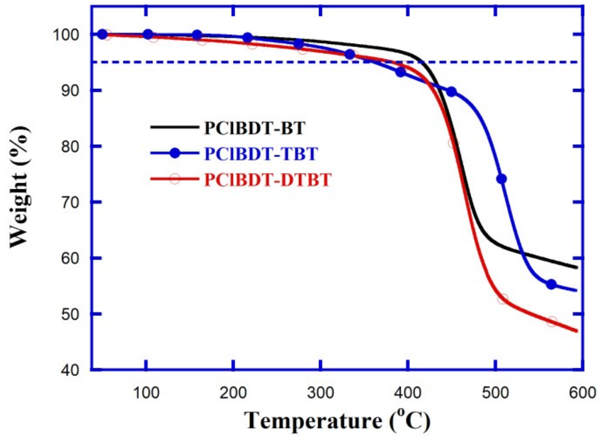

Fig. S9 TGA curves for copolymers PClBDT-BT, PClBDT-TBT and PClBDT-DTBT.

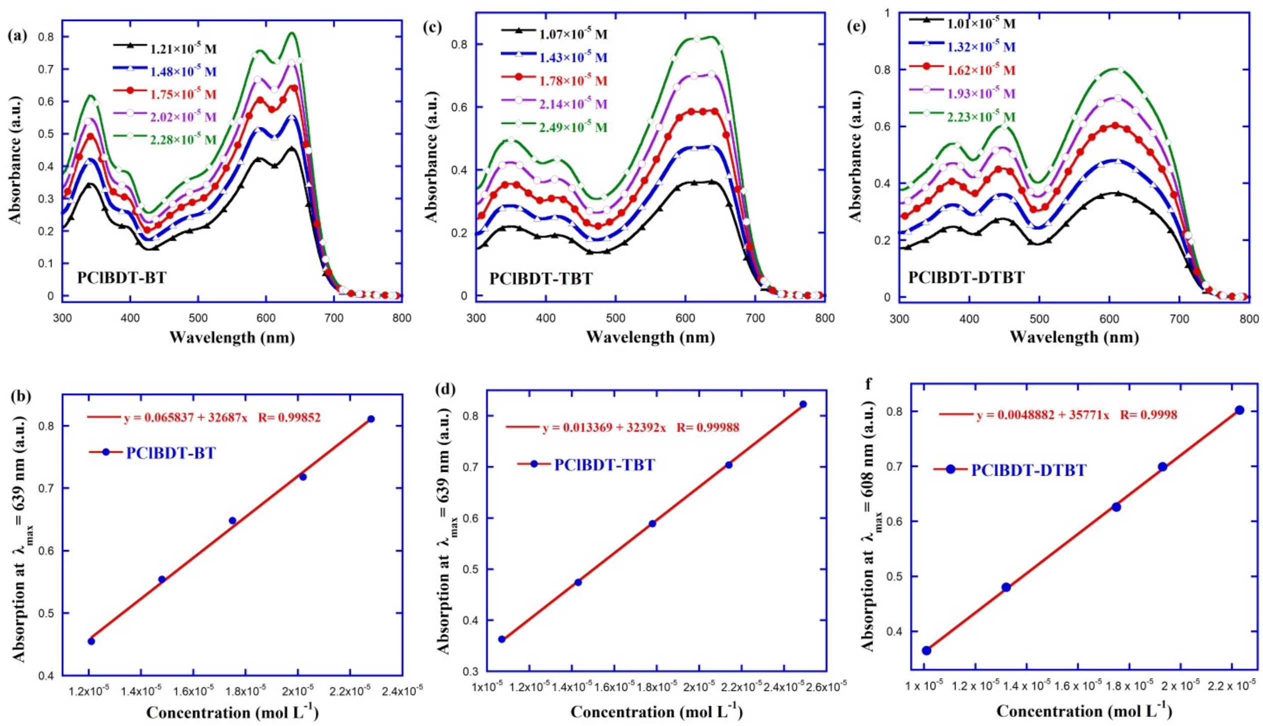

Fig. S10 UV-vis absorption spectra for PClBDT-BT, PClBDT-TBT and PClBDT-DTBT dissolved in solution at varied concentrations and calculation of molar absorption coefficient.

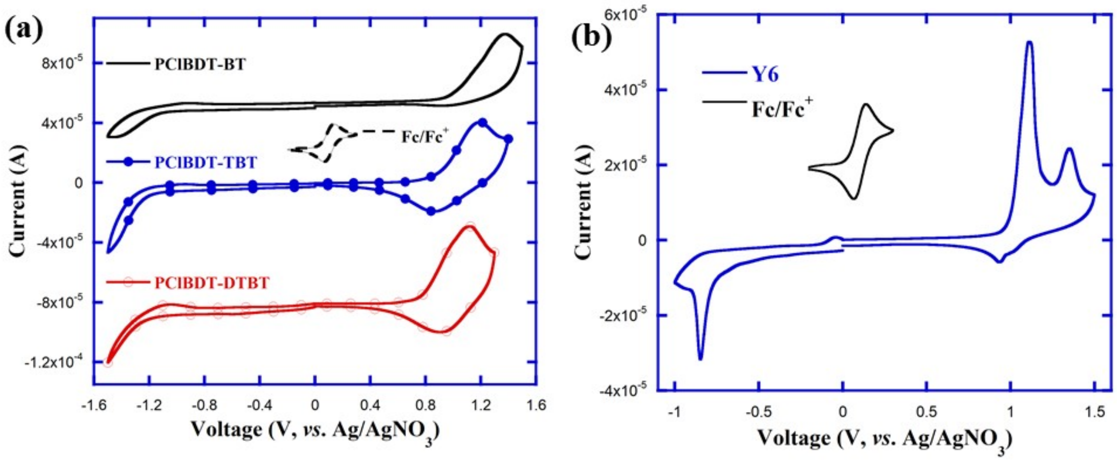

Fig. S11 CV curves for polymer donors (a) and acceptor Y6 (b) under the similar testing condition.

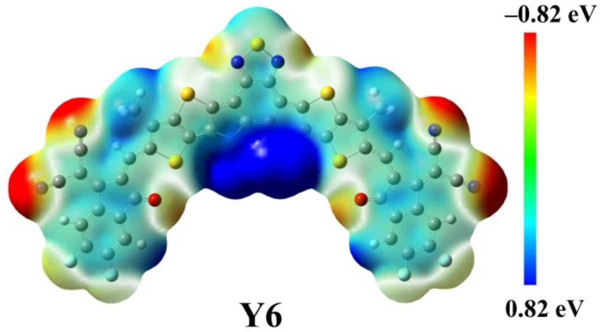

Fig. S12 ESP distribution for Y6.

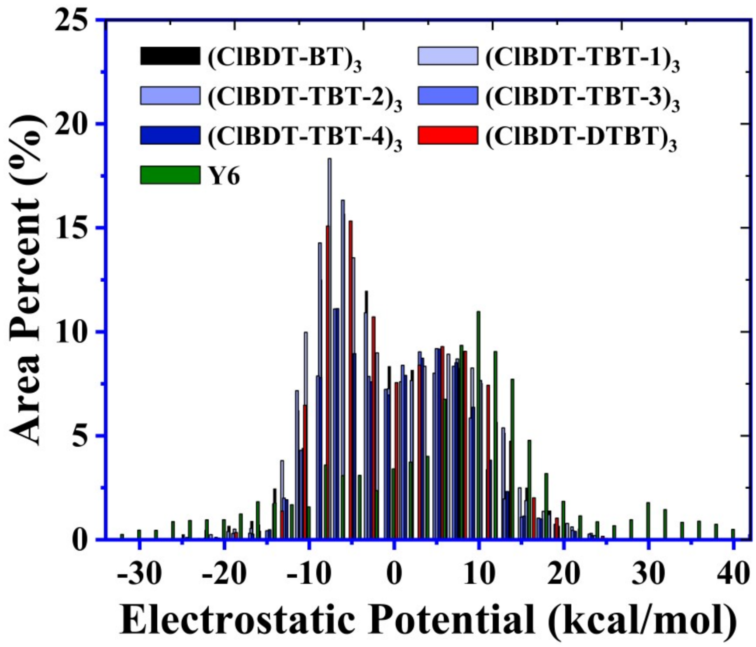

Fig. S13 ESP area distribution for model molecules of donor polymers and acceptor Y6.

Table S3 Dihedral angles of model molecules $(ClBDT\text{-}BT)_3$, $(ClBDT\text{-}TBT\text{-}1)_3$, $(ClBDT\text{-}TBT\text{-}2)_3$, $(ClBDT\text{-}TBT\text{-}3)_3$, $(ClBDT\text{-}TBT\text{-}4)_3$ and $(ClBDT\text{-}DTBT)_3$ through DFT calculation.

Molecule	Structure	Dihedral angle (deg)
$(ClBDT\text{-}BT)_3$	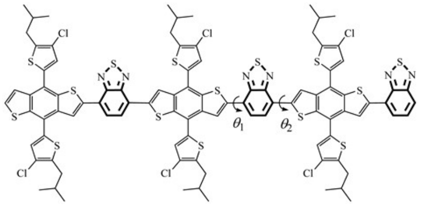	$\theta_1 = -11.48$, $\theta_2 = 7.70$.
$(ClBDT\text{-}TBT\text{-}1)_3$	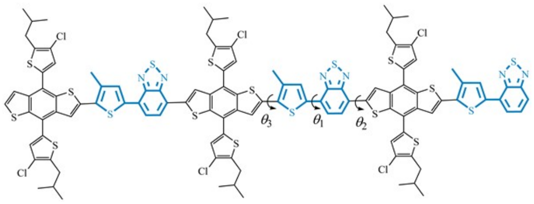	$\theta_1 = 5.48$, $\theta_2 = 8.79$, $\theta_3 = -12.44$
$(ClBDT\text{-}TBT\text{-}2)_3$	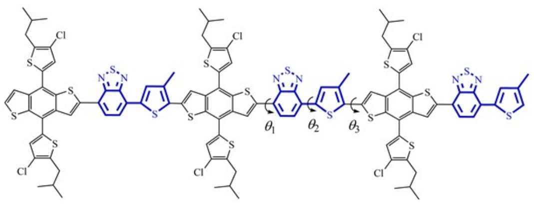	$\theta_1 = -3.81$, $\theta_2 = -1.74$, $\theta_3 = 8.88$
$(ClBDT\text{-}TBT\text{-}3)_3$	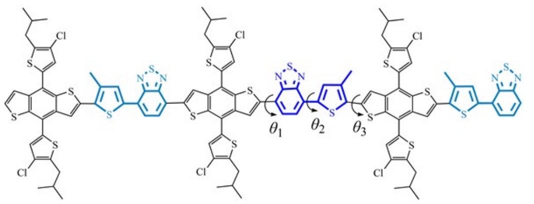	$\theta_1 = -1.17$, $\theta_2 = 0.65$, $\theta_3 = 11.23$
$(ClBDT\text{-}TBT\text{-}4)_3$	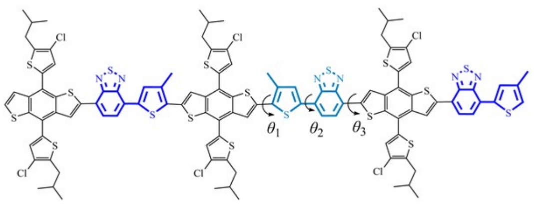	$\theta_1 = -11.89$, $\theta_2 = 2.52$, $\theta_3 = -3.83$
$(ClBDT\text{-}DTBT)_3$	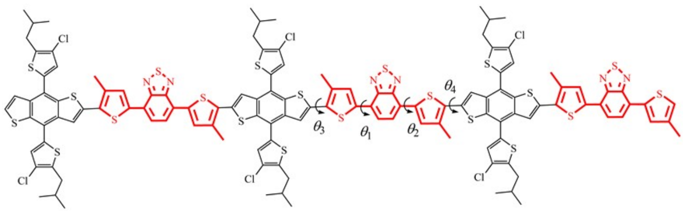	$\theta_1 = 3.13$, $\theta_2 = 3.13$, $\theta_3 = -12.97$, $\theta_4 = -7.18$.

Table S4 Molecular surface area, MPI, extreme ESP value and total average ESP for $(ClBDT\text{-}BT)_3$, $(ClBDT\text{-}TBT\text{-}1)_3$, $(ClBDT\text{-}TBT\text{-}2)_3$, $(ClBDT\text{-}TBT\text{-}3)_3$, $(ClBDT\text{-}TBT\text{-}4)_3$, $(ClBDT\text{-}DTBT)_3$ and Y6.

Molecules	overall surface area (Å^2)	MPI (kcal·mol^{-1})	minimal/maximal values (kcal·mol^{-1})	overall average value (kcal·mol^{-1})
$(ClBDT\text{-}BT)_3$	1444.64	7.13	–26.12/22.66	0.26
$(ClBDT\text{-}TBT\text{-}1)_3$	1703.39	7.16	–26.28/25.35	–0.25
$(ClBDT\text{-}TBT\text{-}2)_3$	1705.22	7.19	–22.67/24.97	–0.25
$(ClBDT\text{-}TBT\text{-}3)_3$	1997.97	6.37	–26.26/24.92	0.02
$(ClBDT\text{-}TBT\text{-}4)_3$	1997.19	6.40	–22.19/24.63	0.16
$(ClBDT\text{-}DTBT)_3$	1967.87	6.99	–21.24/24.57	–0.13
Y6	811.49	11.96	–33.14/41.44	5.49

Table S5 Calculated dipole moments for model molecules $(ClBDT\text{-}BT)_3$, $(ClBDT\text{-}TBT\text{-}1)_3$, $(ClBDT\text{-}TBT\text{-}2)_3$, $(ClBDT\text{-}TBT\text{-}3)_3$, $(ClBDT\text{-}TBT\text{-}4)_3$ and $(ClBDT\text{-}DTBT)_3$.

Polymer	State	X(D)	Y(D)	Z(D)	$\Delta\mu_{g-e}$ (Deby)[a]
$(ClBDT\text{-}BT)_3$	S_0	0.2768	0.8646	0.1879	7.2371
	S_1	–6.95548	1.0015	–0.0403	
$(ClBDT\text{-}TBT\text{-}1)_3$	S_0	–1.4355	–0.7823	0.3626	9.3952
	S_1	7.9158	0.0630	0.0320	
$(ClBDT\text{-}TBT\text{-}2)_3$	S_0	–0.6683	–0.6106	0.5430	8.7782
	S_1	8.0761	–0.0092	0.0640	
$(ClBDT\text{-}TBT\text{-}3)_3$	S_0	–2.8396	–2.5498	2.8608	7.8432
	S_1	–7.8401	0.2210	0.0103	
$(ClBDT\text{-}TBT\text{-}4)_3$	S_0	–2.0084	–1.1782	0.6030	8.0629
	S_1	8.0517	0.4167	0.4279	
$(ClBDT\text{-}DTBT)_3$	S_0	1.0826	0.6803	0.5402	8.1802
	S_1	9.2380	0.2857	0.0395	

[a] $\Delta\mu_{g-e} = [(\mu_{gx}-\mu_{ex})^2 + (\mu_{gy}-\mu_{ey})^2 + (\mu_{gz}-\mu_{ez})^2]^{1/2}$.

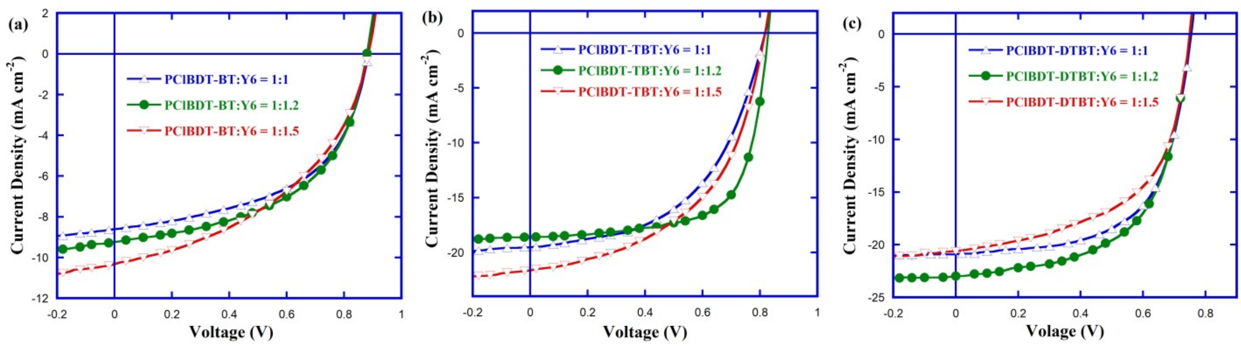

Fig. S14 *J-V* curves for devices under different weight ratio.

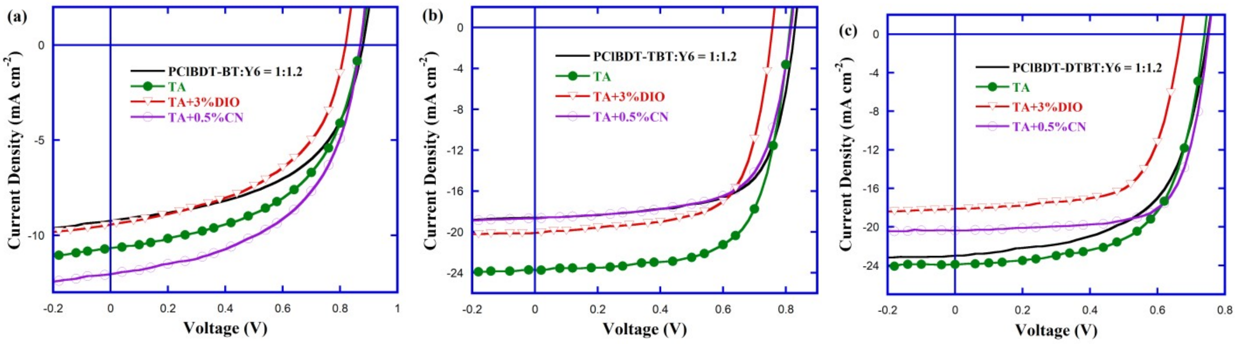

Fig. S15 *J-V* curves for devices using additive and thermal annealing.

Table S6 Photovoltaic performance of devices with different blend ratio, additive or thermal annealing (TA).

Active layer	condition	V_{OC} (V)	J_{SC} (mA·cm^{-2})	*FF* (%)	PCE[a] (%)
PClBDT-BT:Y6	1:1	0.89±0.01	8.61±0.13	53.22±0.51	4.05±0.13
PClBDT-BT:Y6	1:1.2	0.88±0.01	9.23±0.15	52.62±0.53	4.26±0.15
PClBDT-BT:Y6	1:1.5	0.89±0.01	10.32±0.22	44.33±0.48	4.05±0.12
PClBDT-BT:Y6	1:1.2+TA[b]	0.87±0.02	10.67±0.23	52.33±0.52	4.86±0.11
PClBDT-BT:Y6	1:1.2+TA[b]+3%DIO	0.82±0.01	9.44±0.25	50.02±0.50	3.87±0.10
PClBDT-BT:Y6	1:1.2+TA[b]+0.5%CN	0.84±0.01	12.04±0.26	52.88±0.63	5.54±0.13
PClBDT-TBT:Y6	1:1	0.82±0.01	19.52±0.28	51.71±0.52	8.26±0.26
PClBDT-TBT:Y6	1:1.2	0.83±0.01	18.61±0.26	67.54±0.56	10.42±0.28
PClBDT-TBT:Y6	1:1.5	0.82±0.01	21.65±0.29	50.78±0.48	8.99±0.26
PClBDT-TBT:Y6	1:1.2+TA[c]	0.81±0.01	23.72±0.16	67.63±0.54	13.04±0.31
PClBDT-TBT:Y6	1:1.2+TA[c]+3%DIO	0.76±0.02	20.11±0.46	67.07±0.58	10.22±0.25
PClBDT-TBT:Y6	1:1.2+TA[c]+0.5%CN	0.82±0.01	18.68±0.42	66.83±0.53	10.19±0.19
PClBDT-DTBT:Y6	1:1	0.75±0.01	20.90±0.27	62.11±0.49	9.79±0.16
PClBDT-DTBT:Y6	1:1.2	0.75±0.01	22.97±0.29	59.72±0.46	10.29±0.20
PClBDT-DTBT:Y6	1:1.5	0.75±0.01	20.59±0.28	56.51±0.52	8.72±0.17
PClBDT-DTBT:Y6	1:1.2+TA[d]	0.74±0.01	23.88±0.31	62.94±0.75	11.12±0.24
PClBDT-DTBT:Y6	1:1.2+TA[d]+3%DIO	0.67±0.01	18.10±0.33	66.80±0.71	8.10±0.23
PClBDT-DTBT:Y6	1:1.2+TA[d]+0.5%CN	0.75±0.02	20.38±0.27	71.05±0.54	10.89±0.21

[a]Average values of 10 devices. [b]TA at 100 °C for 10 min. [c]TA at 120 °C for 10 min. [d]TA at 110 °C for 10 min.

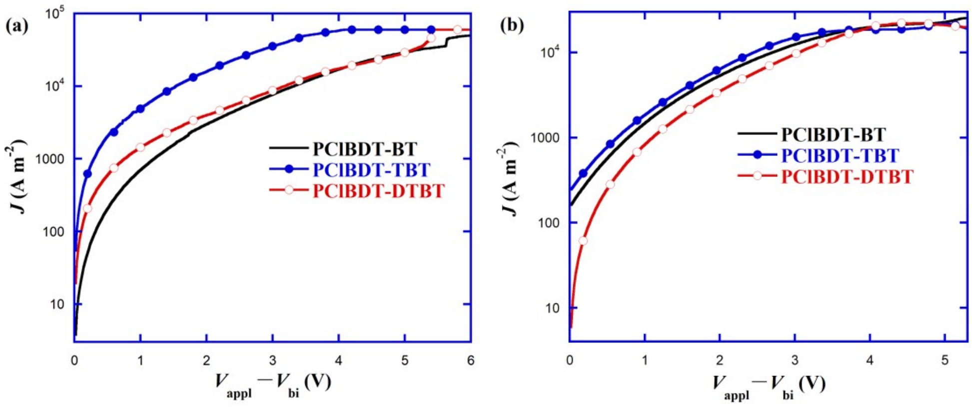

Fig. S16 *J-V* curves of hole-only (a) and electron-only (b) devices under the best fabrication condition.

Table S7 Hole and electron mobilities of the optimized devices measured by SCLC model.

Active layer	Ratios/Additive	Thickness (nm)	k_h/k_e	μ_h/μ_e (cm^2 V^{-1} s^{-1})
PClBDT-BT:Y6	1:1.2/TA+0.5%C	100	17.01/20.96	$1.53\times10^{-4}/8.63\times10^{-5}$
PClBDT-TBT:Y6	1:1.2/TA	120	29.00/28.38	$3.90\times10^{-4}/3.74\times10^{-4}$
PClBDT-	1:1.2/TA	105	28.50/24.60	$3.76\times10^{-4}/2.81\times10^{-4}$

Table S8 Surface tensions (γ) and interaction parameters (χ) for the studied copolymers and Y6.

Polymer	Water (°)	EG(°)	γ(mN/m)	$\chi^{donor\text{-}acceptor}$
Y6	96.8	67.7	29.66	
PClBDT-BT	105.8	77.9	26.04	0.1177K
PClBDT-TBT	103.9	75.9	26.59	0.0838K
PClBDT-DTBT	103.7	75.7	26.36	0.0818K

Table S9 Experimental data obtained from GIWAXS characterization.

Blend film	Out-of-plane (010)				In-plane (100)			
	Location (Å^{-1})	*d*-spacing (Å)	FWHM	CCL (Å)	Location (Å^{-1})	*d*-spacing (Å)	FWHM	CCL (Å)
PClBDT-BT:Y6	1.78	3.52	0.192	29.5	0.27	23.36	0.045	125.7
PClBDT-TBT:Y6	1.83	3.43	0.201	28.1	0.29	21.74	0.052	109.4
PClBDT-DTBT:Y6	1.76	3.57	0.277	20.4	0.27	23.53	0.055	102.8

Reference

1 Y. Lin, F. Zhao, Y. Wu, K. Chen, Y. Xia, G. Li, S. K. K. Prasad, J. Zhu, L. Huo, H. Bin, Z. Zhang, X. Guo, N. Zhang, Y. Sun, F. Gao, Z. Wei, W. Ma, C. Wang, J. Hodgkiss, Z. Bo, O. Inganäs, Y. Li, X. Zhan, *Adv. Mater.*, 2017, **29**, 1604155.

2 Zhang, G. Xu, X. Bi, Z. Ma, W. Tang, D. Li, Y. Q. Peng, *Adv. Funct. Mater.*, 2018, **28**, 1706404.

3 Y. Dong, H. Yang, Y. Wu, Y. Zou, J. Yuan, C. Cui, Y. Li, *J. Mater. Chem. A*, 2019, **7**, 2261–2267.

4 S. Feng, H. Lu, Y. Liu, W. Xue, C. Zhang, H. Zhang, W. Ma, W. Huang, Z. Bo, *ACS Appl. Mater. Interfaces*, **2020**, *12*, 53021−53028.

5 J. Zhao, Y. Li, G. Yang, K. Jiang, H. Lin, H. Ade, W. Ma, H. Yan, *Nat. Energy*, 2016, **1**, 15027.

6 Y. Liu, J. Zhao, Z. Li, C. Mu, W. Ma, H. Hu, K. Jiang, H. Lin, H. Ade and H. Yan, *Nat. Commun.*, 2014, **5**, 5293.

7 J. Yu, P. Chen, C. W. Koh, H. Wang, K. Yang, X. Zhou, B. Liu, Q. Liao, J. Chen, H. Sun, H. Y. Woo, S. Zhang, X. Guo, *Adv. Sci.*, 2019, **6**, 1801743.

8 Z. Chen, Z. Hu, Y. Liang, C. Zhou, J. Xiao, G. Zhang, F. Huang, *Org. Electron.*, **2020**, *85*, 105874.

9 H. Hu, K. Jiang, G. Yang, J. Liu, Z. Li, H. Lin, Y. Liu, J. Zhao, J. Zhang, F. Huang, Y. Qu, W. Ma and H. Yan, *J. Am. Chem. Soc.*, 2015, **137**, 14149−14157.

10 J. Zhang, Y. Li, J. Huang, H. Hu, G. Zhang, T. Ma, P. C. Y. Chow, H. Ade, D. Pan and H. Yan, *J. Am. Chem. Soc.*, 2017, **139**, 16092−16095.

11 S. Zhang, Y. Qin, J. Zhu and J. Hou, *Adv. Mater.*, 2018, **30**, 1800868.

12 L. An, J. Tong, Y. Huang, Z. Liang, J. Li, C. Yang and X. Wang, *Polymers* **2020**, **12**, 368.

13 J. Tong, J. Li, P. Zhang, X. Ma, M. Wang, L. An, J. Sun, P. Guo, C. Yang, Y. Xia, *Polymer*, 2017, **121**, 183–195.

14 X. Guo, N. Zhou, S. J. Lou, J. Smith, D. B. Tice, J. W. Hennek, R. P. Ortiz, J. T. López Navarrete, S. Li, J. Strzalka, L. X. Chen, R. P. H. Chang, A. Facchetti and T. J. Marks, *Nat. Photonics*, 2013, **7**, 825.

15 J. Comyn, *Int. J. Adhes. Adhes.*, 1992, **12**, 145–149.

16 J. Tong, X. Jiang, H. Li, L. An, C. Yang, Y. Huang, P. Guo, Z. Liang, C. Yang, J. Li, Y. Xia, *Opt. Mater.*, 2021, **121**, 111593.

17 L. Yan, Z. Liang, J. Si, P. Gong, Y. Wang, X. Liu, J. Tong, J. Li and X. Hou, *ACS Appl. Mater. Interfaces*, 2022, **14**, 6945–6957.